Electronic Supplementary Information

Experimental Section

Materials and Chemicals

Cobalt nitrate hexahydrate (II) ($Co(NO_3)_2 \cdot 6H_2O$, 99%), 2-methylimidazole (2-MIM, 99%), potassium ferrocyanide ($K_4[Fe(CN)_6] \cdot 3H_2O$, 98%), sodium borohydride ($NaBH_4$, 98%) and ethanol were purchased from Sinopharm Chemical Reagent Co., Ltd. The nickel foam (NF) was purchased from J&K Chemical Technology, and ultrasonic cleaned with 1M HCl (30 min), deionized (DI) water and anhydrous ethanol several times before use. Ruthenium oxide (RuO_2), platinum (Pt/C 20 wt%) and Nafion (5%) were commercially available. All the reagents and solvents are analytical grade, and used without further purification.

Synthesis of ZIF-L nanosheet arrays on NF

Generally, 0.582 g $Co(NO_3)_2 \cdot 6H_2O$ and 1.313 g 2-MIM were dissolved in 40 ml DI water, separately. Then, two solutions were mixed and stirred for 2 min to form a purple mixture. To which, a piece of cleaned NF (2 cm×5 cm) was immersed, and kept static for 4 h at room temperature. Afterwards, the purple ZIF-L nanosheet arrays coated NF was taken out, washed by DI water for several times and dried at 60 ^oC overnight.

Synthesis of hollow Fe-Co PBA on NF

Typically, 0.6 g $K_4[Fe(CN)_6]$ was dissolved in 60 ml DI water, and then the prepared ZIF-L was immersed into the solution. The Fe-Co PBA was obtained thorough an ion exchange process at room temperature for 4 h. The sample was rinsed

by DI water for several times, and dried at 60 °C overnight. For comparison, Fe-Co PBA-2h and Fe-Co PBA-6h were also prepared by the same method except adjusting the ion exchange time to 2 and 6 h, accordingly.

Synthesis of hollow Fe-Co_3O_4 and V_o-Fe-Co_3O_4 on NF

The Fe-Co_3O_4 was obtained by annealing the Fe-Co PBA in air at 300 °C for 2 h with a ramping rate of 10 °C min^{-1}. The Fe-Co_3O_4-2h and Fe-Co_3O_4-6h were obtained by annealing Fe-Co PBA-2h and Fe-Co PBA-6h under the same conditions. To introduce oxygen vacancy, the Fe-Co_3O_4 was immersed into 0.1 M $NaBH_4$ solution for 1 h. Then, the obtained sample was wash by DI water and ethanol for several times, and dried in a vacuum oven at 60 °C overnight.

Synthesis of Co_3O_4 nanosheet arrays on NF

Co_3O_4 nanosheet arrays were obtained by direct calcination of ZIF-L in air at 300 °C for 2 h with a ramping rate of 10 °C min^{-1}.

Preparation of Pt/C and RuO_2 on NF

2 mg commercial RuO_2 or Pt/C powders were dispersed in 500 μL ethanol, 485 μL DI water and 15 μL Nafion, and then it was sonicated for 30 min to obtain a uniform mixture. Finally, the slurry was dripped onto the NF substrate and dried overnight to obtain Pt/C and RuO_2 electrodes.

Characterization

The morphology and microstructure of the electrocatalysts were investigated by scanning electron microscopy (SEM, Nova Nano SEM 450) and transmission electron microscopy (TEM, FEI Tecnai TF20) equipped with energy dispersive X-ray spectroscopy (EDS). X-ray diffraction patterns (XRD) were collected from Bruker AXS D8 Advance X-ray diffractometer with Cu Kα radiation (λ=1.5406 Å). X-ray photoelectron spectroscopy (XPS) measurement was performed on a Thermo Scientific ESCA-Lab-200i-XL spectrometer. Electron paramagnetic resonance (EPR) spectra were recorded with Bruker EPR EMXPLUS 10/12 spectrometer at 100 K. Thermogravimetric analysis (TGA) was performed on NETZSCH STA 2500 with a ramping rate of 10 K min^{-1}.

Electrochemical measurements

CHI 760E electrochemical workstation (Shanghai Chenhua Instrument Co. Ltd.) was used to test the electrochemical performance of as-prepared electrocatalysts. All the measurements were performed by a three-electrode system using 1 M KOH electrolyte, where Hg/HgO and Pt wire were used reference and counter electrodes, respectively. The measured potentials were referred to reversible hydrogen electrode (RHE) as follows:

$$E_{(RHE)}=E_{(Hg/HgO)}+0.059\times pH+0.098 \quad (S1)$$

The linear sweep voltammetry (LSV) curves were recorded at a scan rate of 5 mV s^{-1}, and the polarization curves were compensated with 90% iR. Notably, the chronopotentialmetric curves were presented without iR correction. Tafel plots of the

overpotential vs. the log (current density) were recorded with linear portions at low overpotentials according to following equation

$$\eta = a + b\log j \qquad (S2)$$

where η was the overpotential, b was the Tafel slope, j was the current density and a was the exchange current density.

Electrochemical impedance spectroscopy (EIS) measurements were carried out to obtain the charge transfer resistance (R_{ct}) in the frequency range of 100 kHz to 0.01 Hz with an AC amplitude of 5mV.

To calculate the electrochemical surface area (ECSA) of elecctrocatalysts, cyclic voltammetry (CV) measurements were performed in the non-faradaic potential ranges at different scan rates to obtain the double layer capacitance (C_{dl}). The C_{dl} and ECSA were estimated as follows:

$$C_{dl}=\Delta j/2\upsilon \qquad (S3)$$

$$ECSA=C_{dl}/C_s \qquad (S4)$$

Where Δj was the current density difference between the anode and cathode, υ was the scan rate and C_s was the specific capacitance. The specific capacitance for a flat surface depending on the electrode materials was found to be in a range of 20–60 μF cm^{-2}, and here we assumed a moderate value of 40 μF cm^{-2} for the calculations of ECSA.

Bubbling method which recording data of the rising volume V (mL) of the soap bubble and the total number of charges transferred under constant current (200 mA cm^{-2}) was measured to calculate the Faraday efficiency (FE) as follows:[1]

$$FE=4 * F * V/(1000 * V_m * It) \quad \text{(S5)}$$

Where F was the Faraday constant (96485 C mol^{-1}), V was the volume change of oxygen production (mL) and V_m is the molar volume (molar under normal temperature and pressure, 24.5 L mol^{-1}).

The TOFs (in s^{-1}) for OER were calculated as follows:[2, 3]:

$$TOF = \frac{j\,(\eta)A}{4nF} \quad \text{(S6)}$$

where j (η) was the current density (in A cm^{-2}) at an overpotential of η, A was the geometric testing area of electrode (in cm^2), 4 represented the number of four-electrons transferred during O_2 production, n was the number of surface active sites (in mol), F was the Faraday constant (96485 C mol^{-1}) and n was the moles of metal atoms on the electrode calculated from the loading weight and the molecular weight of the catalysts.

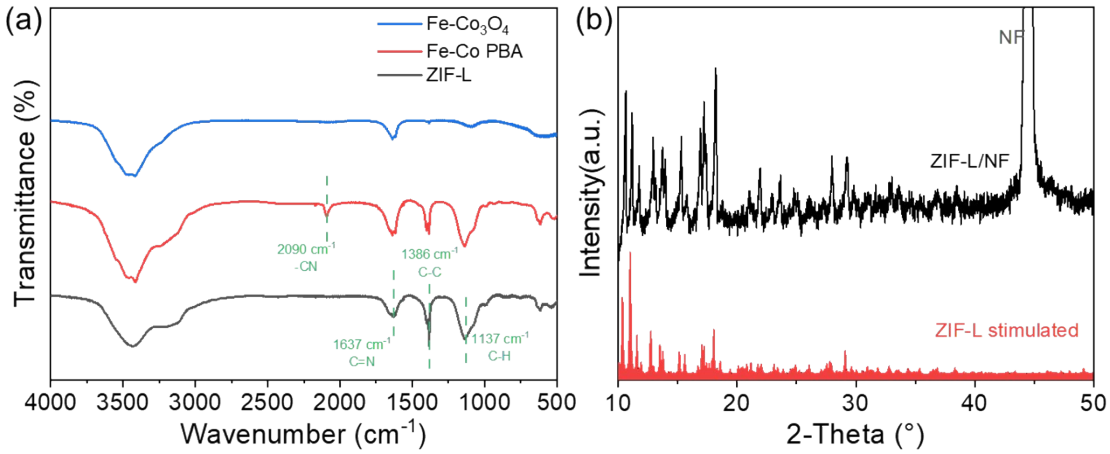

Fig. S1 (a) FT-IR spectra of ZIF-L, Fe-Co PBA and Fe-Co_3O_4. (b) XRD pattern of ZIF-L/NF.

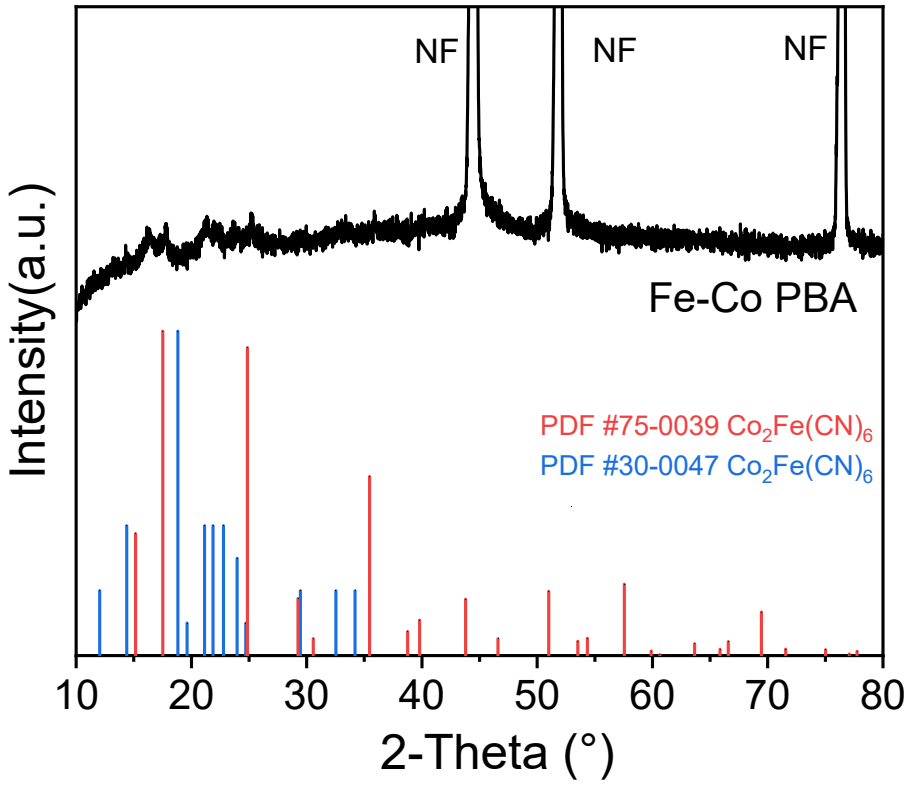

Fig. S2 XRD pattern of Fe-Co PBA.

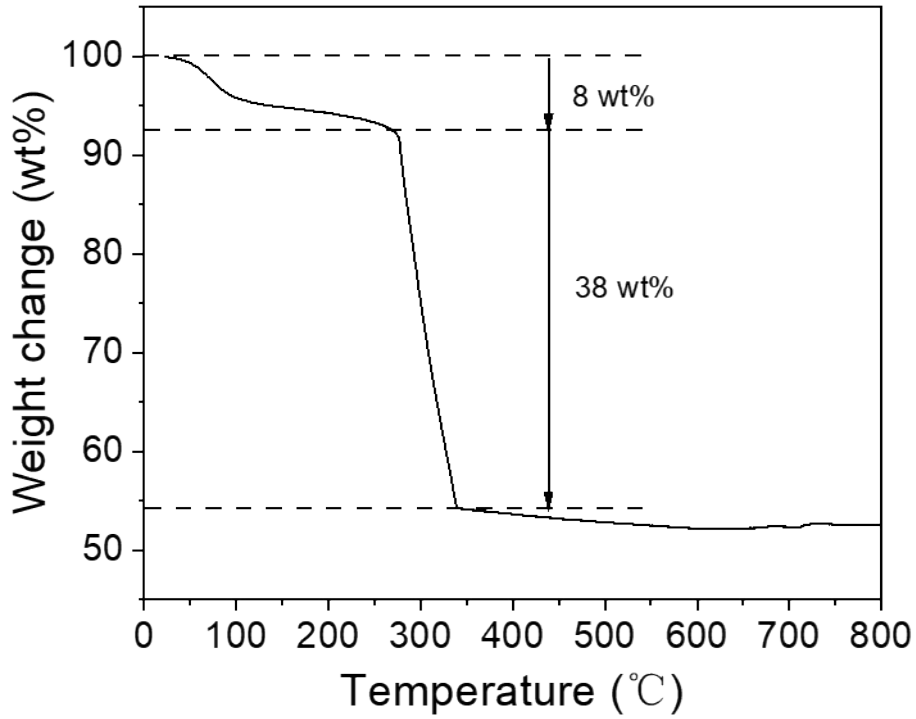

Fig. S3 TG analysis of Fe-Co PBA in air atmosphere.

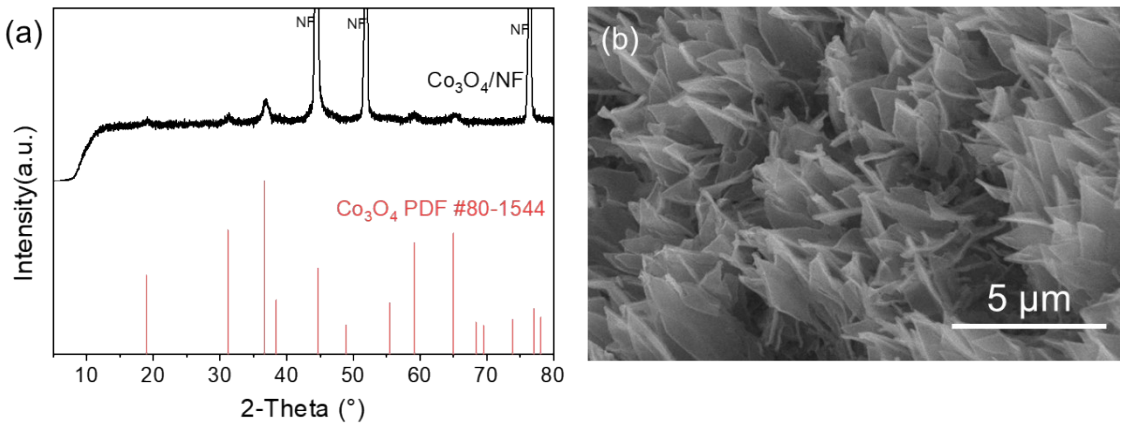

Fig. S4 (a) XRD pattern and (b) SEM image of Co_3O_4/NF.

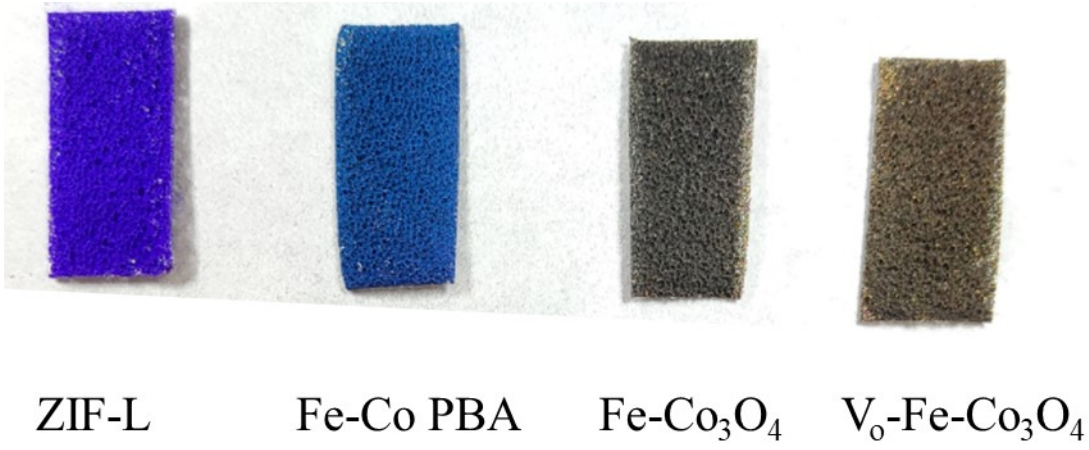

Fig. S5 Optical photographs of the ZIF-L, Fe-Co PBA, Fe-Co_3O_4 and V_o- Fe-Co_3O_4 growing on the nickel foam substrate.

clea

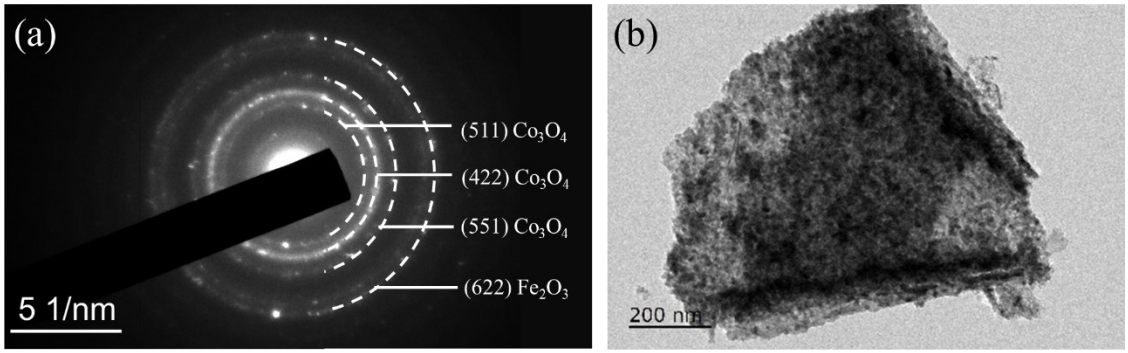

Fig. S6 (a) SAED pattern of V_o-Fe-Co_3O_4; (b) TEM image of V_o-Fe-Co_3O_4.

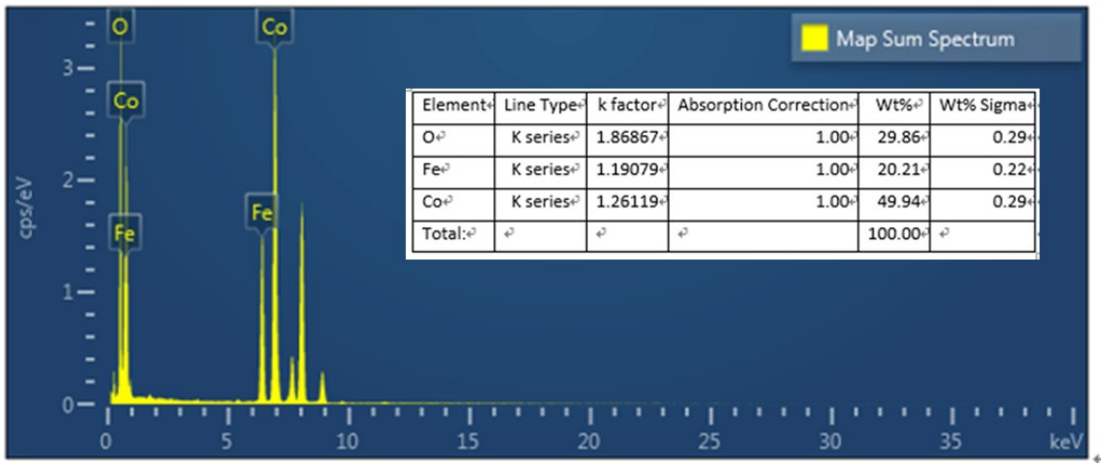

Element	Line Type	k factor	Absorption Correction	Wt%	Wt% Sigma
O	K series	1.86867	1.00	29.86	0.29
Fe	K series	1.19079	1.00	20.21	0.22
Co	K series	1.26119	1.00	49.94	0.29
Total:				100.00	

Fig. S7 EDS pattern of of V_o-Fe-Co_3O_4 and corresponding compositions of the sample.

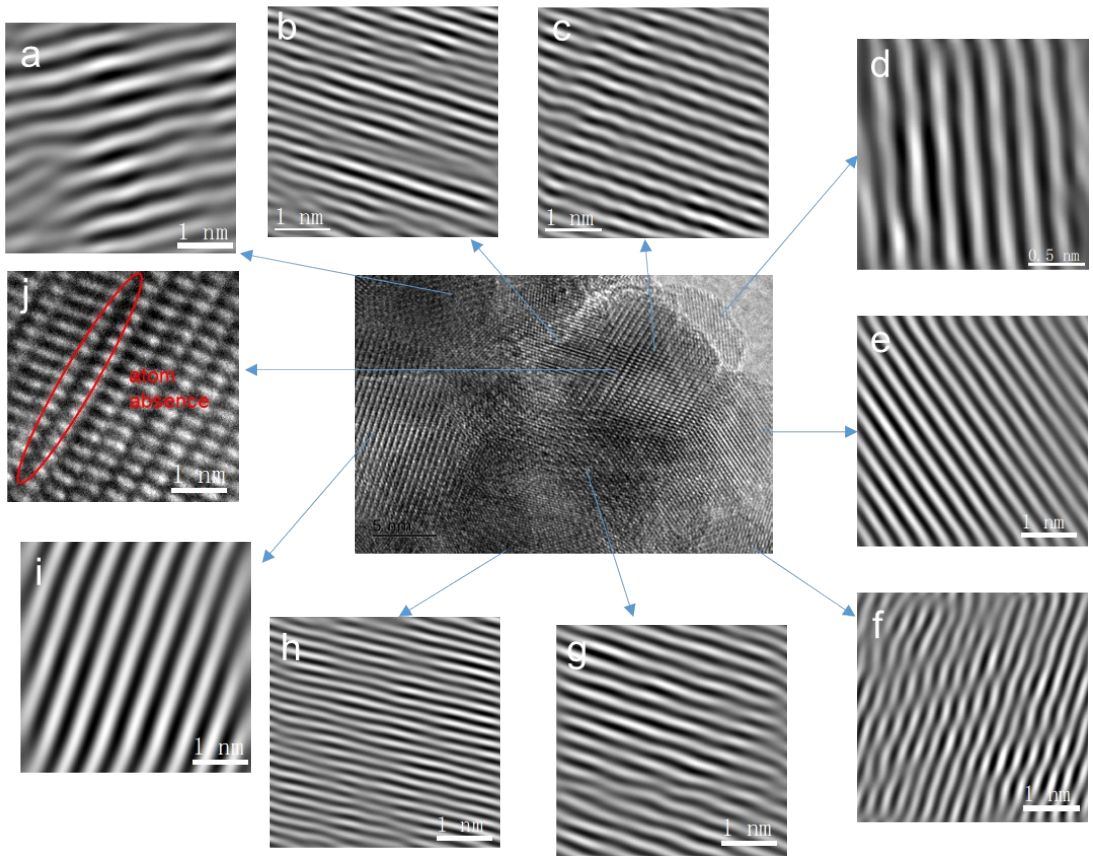

Fig. S8 HRTEM images of V_o-Fe-Co_3O_4 at different positions.

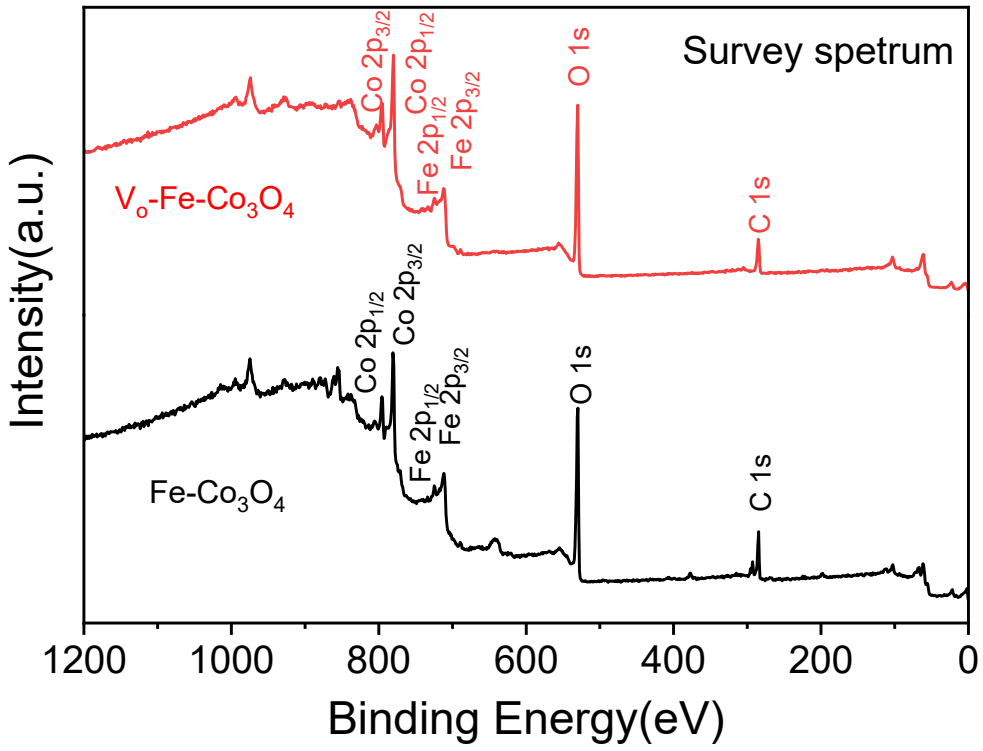

Fig. S9 Survey spectrum of V_o-Fe-Co_3O_4 and Fe-Co_3O_4.

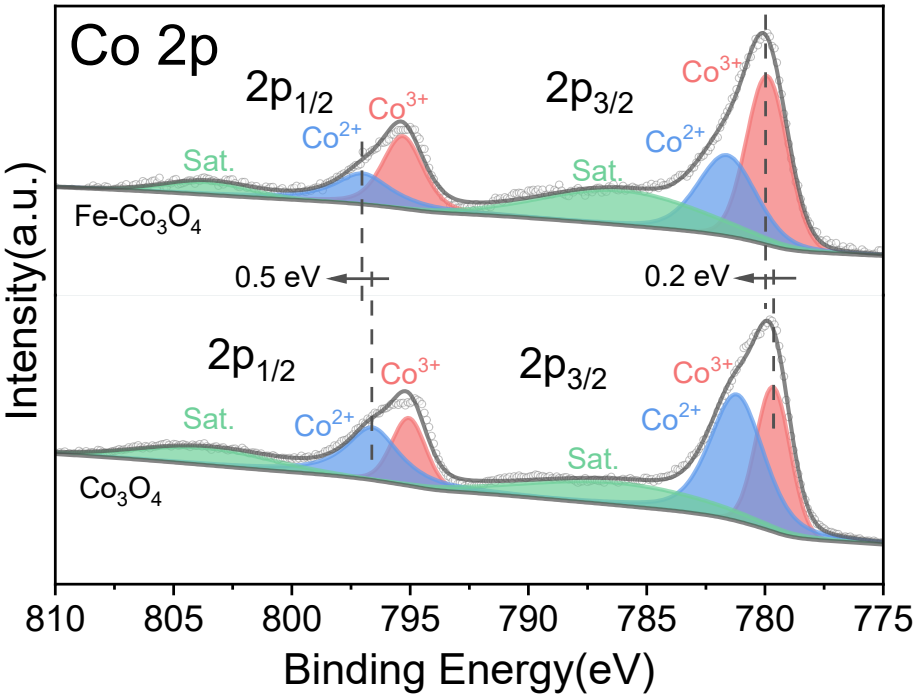

Fig. S10 High resolution XPS spectra of Co 2p of Fe-Co_3O_4 and Co_3O_4.

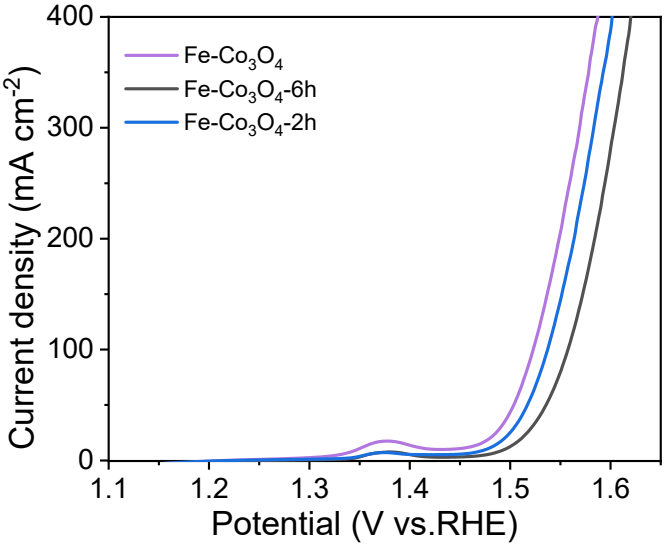

Fig. S11 OER polarization curves of the samples prepared with different ion exchange times.

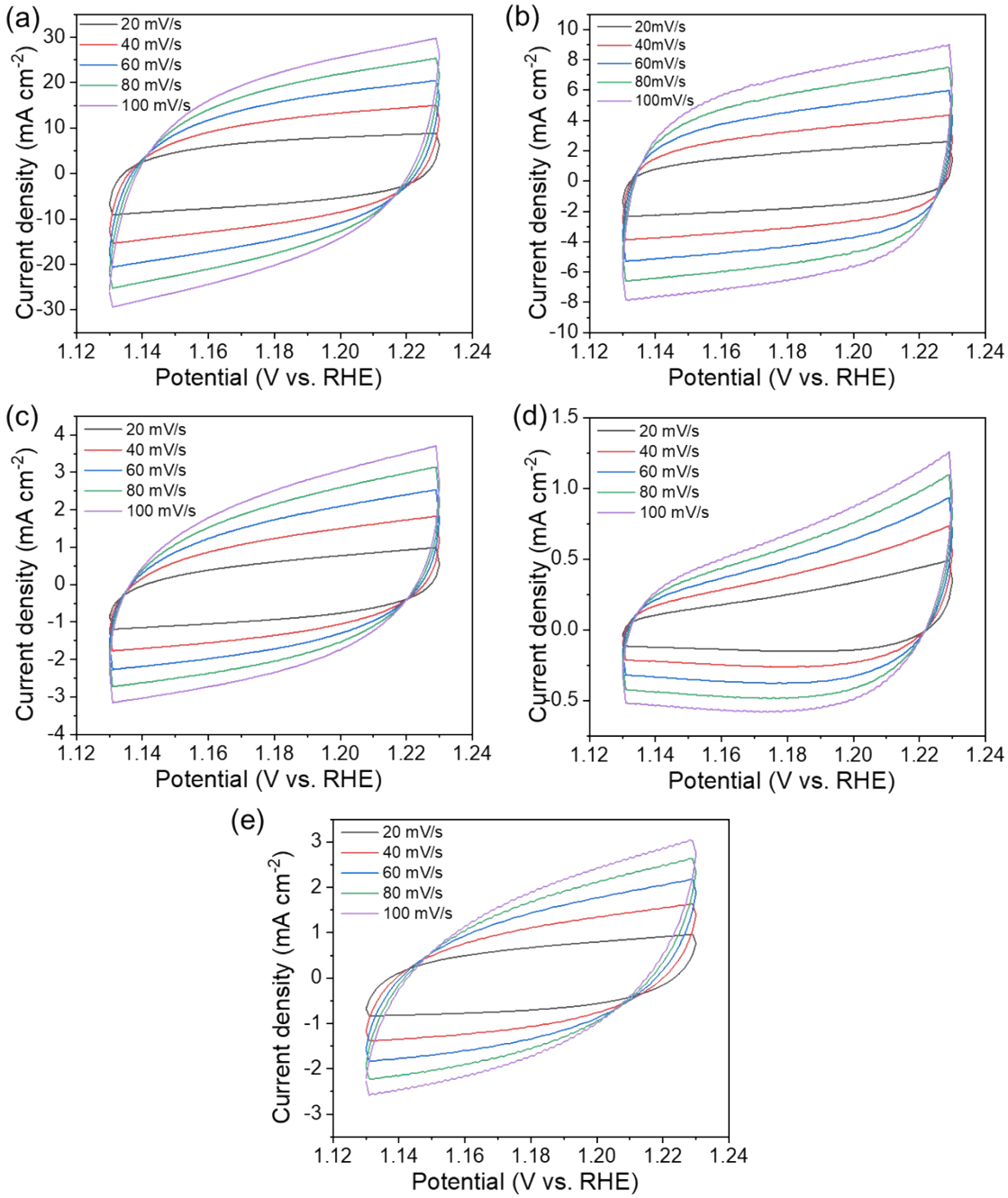

Fig. S12 CV curves of (a) V_o-Fe-Co_3O_4, (b) Fe-Co_3O_4, (c) Co_3O_4, (d) NF and (e) RuO_2 in the non-faradaic regions.

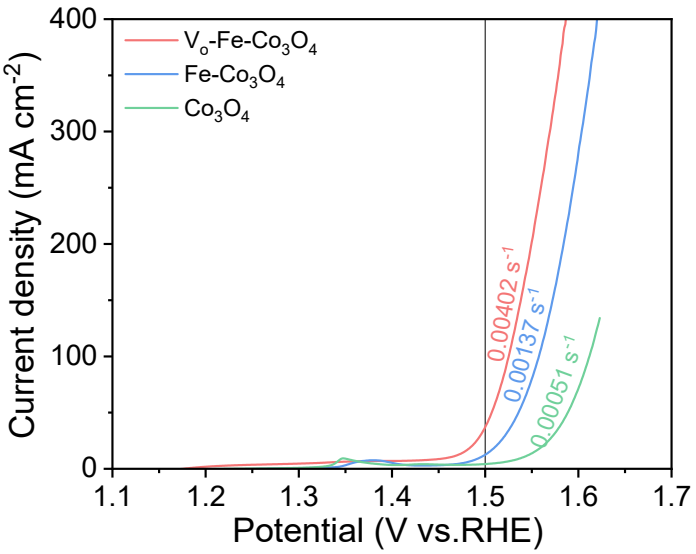

Fig. S13 TOF values of V_o-Fe-Co_3O_4, Fe-Co_3O_4 and Co_3O_4 at the overpotential of 270 mV.

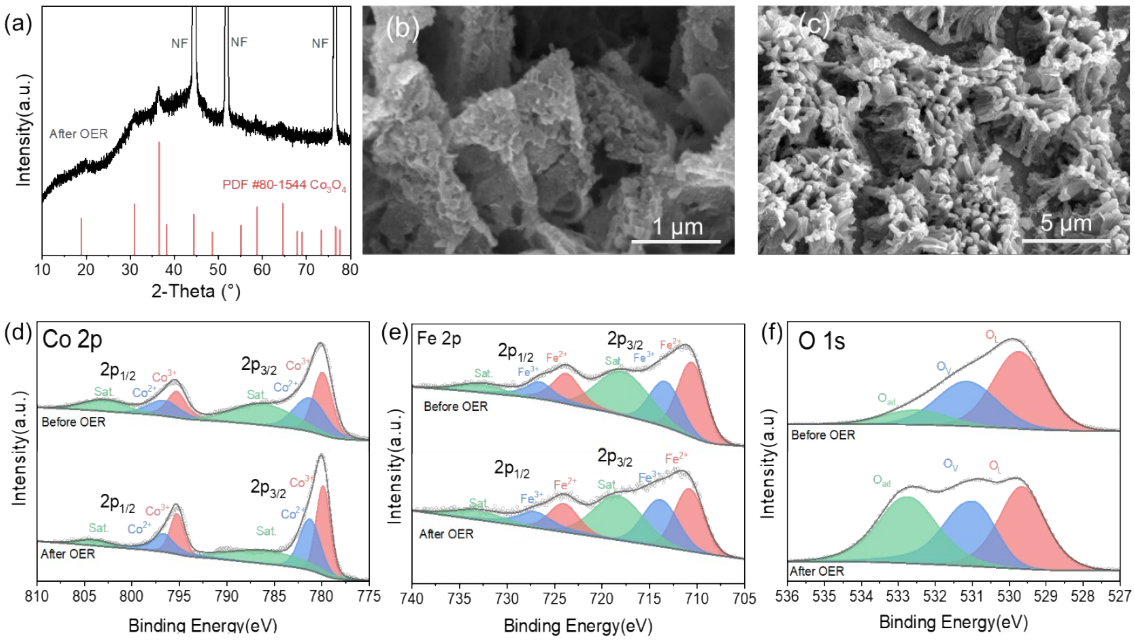

Fig. S14 (a) XRD pattern and (b, c) SEM images of V_o-Fe-Co_3O_4 after 50 h CP test toward OER. High resolution XPS spectra of (d) Co 2p, (e) Fe 2p and (f) O 1s of V_o-Fe-Co_3O_4 before and after 50 h CP test toward OER.

Table S1 EIS results of V_o-Fe-Co_3O_4, Fe-Co_3O_4, Co_3O_4, NF and RuO_2.

	V_o-Fe-Co_3O_4	Fe-Co_3O_4	Co_3O_4	NF	RuO_2
R_s (Ω)	1.18	1.17	1.52	1.29	1.23
R_{ct} (Ω)	2.30	3.60	6.98	10.01	3.69

Table S2 Comparison of various catalysts for OER in 1 M KOH electrolyte.

Catalysts	η_{10} (mV)	Tafel slope (mV dec^{-1})	Reference
B-CoO/Co@NC/NF	307	65.2	[4]
Co_2P–Co_3O_4/C	246	69.5	[5]
$NiCoO_x$-CN	326	70.8	[6]
Zn-doped Co_3O_4	370	63	[7]
Fe_2O_3/$ZnCo_2O_4$	261	71.8	[8]
Ru/Co_3O_{4-x}	280	86.9	[9]
Fe-Co_3O_4 NS/CC	290	67.9	[10]
$CoSe_2$/$FeSe_2$ DS-HNCs	240	44	[11]
$Fe_xCo_{3-x}O_4$/NF	327(η_{20})	57	[12]
$(Ni,Fe)_2P$/C HNRs	258	45.5	[13]
Fe−CoSe PA	285	68	[1]
Fe–CoP HTPAs	230	43	[14]
hollow Fe-CoP prism	236	32.9	[15]
Co_3O_4/Co-Fe oxide DSNBs	297	61	[16]
V_o-Fe-Co_3O_4	**223**	**57.4**	**This work**

Reference

1. J. Li, Q. He, Y. Lin, L. Han and K. Tao, *Inorganic Chemistry*, 2022, **61**, 19031.
2. C. Wang and L. Qi, *Angewandte Chemie International Edition*, 2020, **59**, 17219.
3. H. Yang, H. Sun, X. Fan, X. Wang, Q. Yang and X. Lai, *Materials Chemistry Frontiers*, 2021, **5**, 259.
4. D. C. Cha, T. I. Singh, A. Maibam, T. H. Kim, D. H. Nam, R. Babarao and S. Lee, *Small*, 2023, **19**, 2301405.
5. G. Huang, M. Hu, X. Xu, A. A. Alothman, M. S. S. Mushab, S. Ma, P. K. Shen, J. Zhu and Y. Yamauchi, *Small Structures*, 2023, **4**, 2200235.
6. X. Wang, Y. Dai, P. Wang and D. Yue, *International Journal of Hydrogen Energy*, 2023, DOI: 10.1016/j.ijhydene.2023.07.292, 0360-3199.
7. Y. Yang, L. Xu, W. Wang, R. Han, J. Ma, M. Yao, S. Geng and F. Liu, *Journal of Materials Science*, 2023, **58**, 5234.
8. S. Fu, Y. Ma, X. Yang, X. Yao, Z. Jiao, L. Cheng and P. Zhao, *Applied Catalysis B: Environmental*, 2023, **333**, 122813.
9. C.-Z. Yuan, S. Wang, K. San Hui, K. Wang, J. Li, H. Gao, C. Zha, X. Zhang, D. A. Dinh, X.-L. Wu, Z. Tang, J. Wan, Z. Shao and K. N. Hui, *ACS Catalysis*, 2023, **13**, 2462.
10. Y. Li, W. Zhu, X. Fu, Y. Zhang, Z. Wei, Y. Ma, T. Yue, J. Sun and J. Wang, *Inorganic Chemistry*, 2019, **58**, 6231.
11. C. Xu, Q. Li, J. Shen, Z. Yuan, J. Ning, Y. Zhong, Z. Zhang and Y. Hu, *Nanoscale*, 2019, **11**, 10738.
12. T. I. Singh, G. Rajeshkhanna, S. B. Singh, T. Kshetri, N. H. Kim and J. H. Lee, *ChemSusChem*, 2019, **12**, 4810.
13. S. K. Ramesh, J. Son, V. Ganesan and J. Kim, *Nanoscale*, 2022, **14**, 16262.
14. E. Hu, J. Ning, D. Zhao, C. Xu, Y. Lin, Y. Zhong, Z. Zhang, Y. Wang and Y. Hu, *Small*, 2018, **14**, 1704233.
15. X. Ding, H. Huang, Q. Wan, X. Guan, Y. Fang, S. Lin, D. Chen and Z. Xie, *Journal of Energy Chemistry*, 2021, **62**, 415.
16. X. Wang, L. Yu, B. Y. Guan, S. Song and X. W. D. Lou, *Advanced Materials*, 2018, **30**, 1801211.